Title

Computationally efficient modeling strategy for evaporator performance under frost conditions

Authors

Kim, Donghun
Braun, James E
Ramaraj, Sugirdhalakshmi

Publication Date

2018-12-01

DOI

10.1016/j.ijrefrig.2018.09.004

Peer reviewed

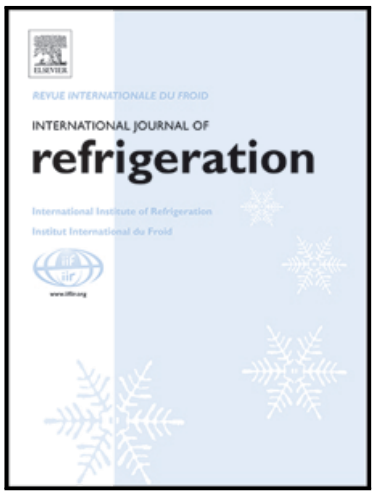

Computationally Efficient Modeling Strategy for Evaporator Performance under Frost Conditions

Donghun Kim, James E. Braun, Sugirdhalakshmi Ramaraj

PII: S0140-7007(18)30326-8
DOI: https://doi.org/10.1016/j.ijrefrig.2018.09.004
Reference: JIJR 4097

To appear in: *International Journal of Refrigeration*

Received date: 27 April 2018
Revised date: 24 July 2018
Accepted date: 3 September 2018

Please cite this article as: Donghun Kim, James E. Braun, Sugirdhalakshmi Ramaraj, Computationally Efficient Modeling Strategy for Evaporator Performance under Frost Conditions, *International Journal of Refrigeration* (2018), doi: https://doi.org/10.1016/j.ijrefrig.2018.09.004

Highlights

- A numerically efficient but accurate model for frosting evaporators is developed.
- The enthalpy-based reformulation and linearization method are employed
- Simulation results on flat plate and finned-tube heat exchangers are provided.
- It is 8 to 20 times faster than reference models but withcomparable accuracy.

Computationally Efficient Modeling Strategy for Evaporator Performance under Frost Conditions

Donghun Kim[a,*], James E. Braun[a], Sugirdhalakshmi Ramaraj[a]

[a]*Ray W. Herrick Laboratories, School of Mechanical Engineering, Purdue University, West Lafayette, IN, USA*

Abstract

Growth of a frost layer on an evaporator surface due to low evaporator temperature as well as moisture contained in surrounding air deteriorates performance of a refrigeration system significantly and requires significant energy for defrost. Many studies have been performed to model the heat and mass transfer phenomena in an attempt to have insight and accurate prediction. However, many models form nonlinear algebraic differential equations which require iterative numerical solvers. Computationally efficient but accurate models are needed in order to evaluate overall system performance. The objective of this paper is to introduce a modeling approach to overcome the problem. A solution strategy based on an enthalpy-based reformulation and linearization method will be presented. Comparisons of the proposed and detailed model results for both flat plate and finned tube heat exchangers are provided. The proposed modeling approach is around 10 times faster than reference models while maintaining comparable accuracy.

Keywords: `frost modeling, frosting evaporator, heat exchanger, defrost`

1. INTRODUCTION

Frost accumulation on a cold evaporator surface occurs when moist air flows over the surface. This can significantly deteriorate performance of a refrigeration unit due to the increase of thermal resistance of frost and decrease of air flow rate associated with frost built-up. A number of models have been developed for accurately predicting the frost growth on refrigeration system evaporators. Jones and Parker [1] developed a one-dimensional model to predict dynamic responses of a frost layer on a cold plate. The model is based on the assumption that the amount of water vapor being frozen is uniform in a frost layer and they arrived at a nonlinear algebraic equation that has to be solved at each time step.

*Corresponding author
Email address: `kim1077@purdue.edu` (Donghun Kim)

Kondepudi and O'Neal [2] developed a finned-tube heat exchanger model under frosting conditions. An energy transfer coefficient, which is a generalization of an overall heat transfer coefficient for dry conditions, was introduced and the ϵ-NTU method was applied. Lee et. al. [3] developed a model for a flat plate based on the assumption of a homogeneous absorption of water vapor in a frost layer. Analytic solutions for distributions of temperature and water vapor density in a frost layer were derived. A total heat flux and frost surface temperature are calculated iteratively with an air side heat transfer equation. The same methodology has been applied to a finned tube heat exchanger and results of the proposed model agreed well with experimental data [4]. Tso et. al. [5] investigated spatial distributions of the air temperature, frost growth rate and densification rate for a finned tube heat exchanger. For each control volume, the analytic solution of [3] was coupled to the energy equation for a frost layer and the air side heat transfer equation. A similar study has been carried out by Padhmanabhan et. al. [6] to predict an evolution of a non-uniform frost thickness distribution under fixed flow conditions. The modeling approach of [1] for a frost layer was adopted. Silva et. al. [7] studied interactions between a finned tube heat exchanger and fixed speed fan, and corresponding transient behaviors of the cooling capacity and frost growth. A frosting evaporator model was iterated with a fan characteristic curve for the purpose.

Most of models, even for one-dimensional heat transfer, form nonlinear algebraic differential equations and thereby iterative numerical methods are needed for each time step and control volume (see above and other papers [8, 9, 10, 11]). Therefore, it is computationally demanding to use them for other purposes, e.g. defrost control evaluations.

This paper aims at developing a numerically efficient modeling approach, that is generally applicable to models which include a water vapor diffusion equation, to overcome this problem. It is based on an enthalpy-based reformulation and linearization method. Baseline models are selected and described in Section 2. Section 3 shows our modeling approach based on the reference models. Comparisons of the proposed and reference model results are provided in Section 4.

2. DESCRIPTIONS OF REFERENCE MODELS

This section is to introduce two reference modeling approaches for a frosting evaporator that are used to develop and benchmark our simplified modeling approach. We select Lee's [3] and Jones and Parker's [1] models as our baseline models, because they are theoretical, experimentally validated, and widely used in the literature over the past several decades, e.g. [5, 4, 7, 8, 9, 10, 11].

For simplicity in understanding the basic modeling approaches, consider a flat plate where the temperature is fixed as T_p. Fig. 1 shows a control volume for a frost layer of width dx where mass and energy balances are applied and where y measures the distance from the plate surface into the frost layer. q''_{tot}

is the total energy heat flux from the air to the frost layer and is given by

$$q''_{tot} = \alpha(T_a - T_\delta) + h_{sub}\alpha_d(\omega_a - \omega_{v,sat}(T_\delta)). \quad (1)$$

The following assumptions were commonly employed in reference models.

- frost surface temperature in each control volume is lower than freezing point
- heat and mass transfer within the frost layer are one dimensional and quasi-steady
- water vapor is saturated at the frost surface and within the frost layer (thermal equilibrium)
- thermal conductivity of the frost layer varies only with frost density
- diffusion coefficient of water vapor is uniform
- uniform frost density

For simplicity of notation, time dependency of variables is omitted in most equations in this paper.

2.1. Lee's model

To describe the water vapor diffusion and absorption phenomena in a frost layer, Lee [3] additionally assumed that the amount of water vapor being frozen is proportional to the local water vapor density. We call Lee's model a homogeneous first-order ice formation model. The term "homogeneous" is to indicate that the water vapor absorption occurs at all locations of a frost layer rather than just at the interface between the air and the frost layer. The term "first order" is to point out that the amount of water vapor being frozen is proportional to the local water vapor density (see the r.h.s. of Eqn. 2).

Using the assumptions, the governing equations and boundary conditions for a given control volume of width dx at a time are

$$D\frac{d^2\rho_v}{dy^2} = \kappa\rho_v, \quad (2)$$

$$-k_{fr}\frac{d^2T}{dy^2} = h_{sub}\kappa_r\rho_v \quad (3)$$

and

$$\frac{d\rho_v}{dy}(0) = 0, \;\; \rho_v(0) = \rho_{v,sat}(T_p) \quad (4)$$

$$k_{fr}\frac{dT}{dy}(\delta) = q''_{tot} - h_{sub}D\frac{d\rho_v}{dy}(\delta), \;\; T(0) = T_p. \quad (5)$$

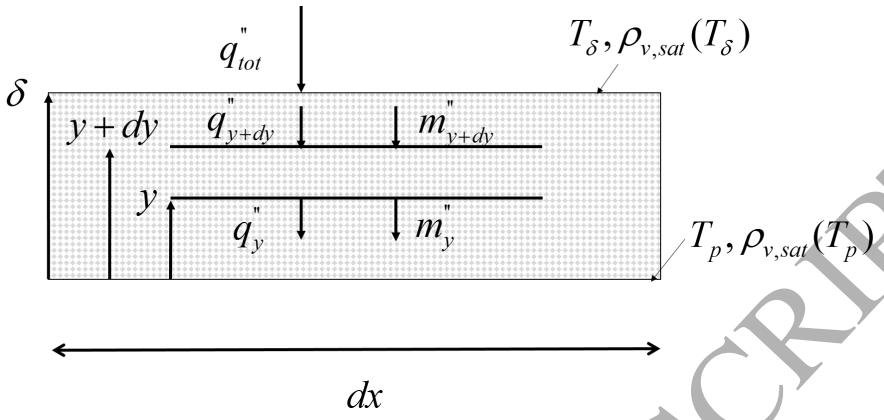

Figure 1: Schematic diagram in a frost layer

Corresponding solutions for Eqn. 2 and 3 are (See [3])

$$\rho_v(y) = \rho_{v,sat}(T_p)\cosh(My), \tag{6}$$

$$T(y) = T_p + \frac{q''_{tot}}{k_{fr}}y - \frac{\kappa h_{sub}\rho_{v,sat}(T_p)}{k_{fr}M^2}(\cosh(My) - 1) \tag{7}$$

where $M = \sqrt{\kappa/D}$.

The water vapor absorption coefficient can be calculated by imposing a boundary condition, i.e. $\rho_v(\delta) = \rho_{v,sat}(T_\delta)$, as follows.

$$\kappa = \frac{D}{\delta^2}[\cosh^{-1}(\frac{\rho_{v,sat}(T_\delta)}{\rho_{v,sat}(T_p)})]^2. \tag{8}$$

From Eqn. 7,

$$T_\delta = T_p + \frac{q''_{tot}}{k_{fr}}\delta - \frac{\kappa h_{sub}\rho_{v,sat}(T_p)}{k_{fr}M^2}(\cosh(M\delta) - 1). \tag{9}$$

Note that, to calculate the temperature at the surface of the frost layer, i.e. T_δ, based on a local inlet air condition (T_a, ω_a) and a plate temperature T_p, Eqn. 1 and 9 must be solved iteratively using Eqn. 8 and psychrometric relations. Once T_δ is obtained, the mass flux of water vapor from the air to frost surface and densification rate are obtained by the equations of the air side mass transfer and $D\frac{d\rho_v}{dy}(\delta)$ respectively as given by

$$m''_{fr} = \alpha_d(\omega_a - \omega_{v,sat}(T_\delta)) \tag{10}$$

and

$$m''_\rho = DM\rho_{v,sat}(T_\delta)tanh(M\delta). \tag{11}$$

Using those, the frost thickness and density are updated for the next time step as follows

$$\begin{aligned} \delta(t+\Delta t) &= \delta(t) + \frac{1}{\rho_{fr}}(m_{fr}^{''}(t) - m_{\rho}^{''}(t))\Delta t \\ \rho_{fr}(t+\Delta t) &= \rho_{fr}(t) + \frac{1}{\delta}m_{\rho}^{''}(t)\Delta t. \end{aligned} \tag{12}$$

The air temperature and humidity at the exit of the control volume are calculated using energy and water vapor mass balances. The exit condition becomes the inlet condition for the next control volume. The above procedure is repeated for a predefined simulation period.

2.2. Jones and Parker's model

The Jones and Parker [1] approach differs from Lee's in modeling the absorption rate of water vapor. More precisely, Jones and Parker assumed that the amount of water vapor being frozen is the same at all locations in the frost layer in contrast to Lee's assumption. This results in the following diffusion and energy equations in the frost layer[1].

$$D\frac{d^2\rho_v}{dy^2} = m_{\rho}^{''}/\delta \tag{13}$$

and

$$-k_{fr}\frac{d^2T}{dy^2} = h_{sub}m_{\rho}^{''}/\delta. \tag{14}$$

Since the water vapor absorption rate or ice formation rate on the right hand side of Eqn. 13 is independent of location y, we call Jones and Parker's model a homogeneous zeroth order ice formation model.

The final equation of Jones and Parker's model is

$$T_{\delta} = -\left(D\frac{d\rho_{v,sat}}{dT}(T_{\delta}) \times \frac{q_{tot}^{''}}{k_{fr} + h_{sub}D\frac{d\rho_{v,sat}}{dT}(T_{\delta})}\right) \times \frac{h_{sub}}{2k_{fr}}\delta + \frac{q_{tot}^{''}}{k_{fr}}\delta + T_p. \tag{15}$$

The original expression in the reference paper (See Eqn. (14A) in [1]) is a bit more complicated than Eqn. 15 due to the inclusion of the ideal gas law for water vapor and the expansion of the effective diffusivity D using correlations of porosity and tortuousity for the frost layer, but it is equivalent to Eqn. 15.

Eqn. 15 together with the air side heat and mass transfer equation, i.e. Eqn. 1, forms a very complicated implicit equation which must be solved by algebraic equation solvers.

[1] See Eqn. (8A,9A) in the reference paper [1].

3. SIMPLIFIED MODEL DEVELOPMENT

A numerical strategy to avoid iteration consists of the following two main steps.

1. Reformulate Eqn. 1 with an approximation such that q''_{tot} relies on a difference in enthalpy rather than two differences of temperature and humidity.
2. Reformulate the reference models, i.e. Eqn. 9 and Eqn. 15, and linearly approximate q''_{tot} with respect to the enthalpy potential.

3.1. Reformation of air side heat equation using enthalpy potential

The main idea for the first step comes from the enthalpy potential approach. This approach for modeling combined heat and mass transfer was developed several decades ago and has been validated for and widely applied to cooling coils, cooling towers, and desiccant wheels. It is very well accepted as a general approach for characterizing total energy transfer due to the combined effects of temperature and humidity gradients in air and is introduced in a number of HVAC equipment modeling text books [12, 13]. The enthalpy potential formulation has also been used for modeling frost formation on evaporators [2, 14]. The current paper extends the previous work by integrating this generalized enthalpy potential approach into an overall computationally-efficient evaporator model.

Let us define the following quantity for moist air.

$$i(T,\omega) := h(T,\omega) + \omega \times (h_{sub} - h_v^{ref}) \qquad \forall T,\omega \tag{16}$$

where h_v^{ref} represents the specific enthalpy of moist air used in developing the psychrometric chart (ASHRAE [15]). More precisely, $h(T,\omega) = (C_{p,a}+C_{p,v}\omega)\times T + h_v^{ref}\omega$ and h_v^{ref} is the specific enthalpy of saturated water vapor at 0 (^oC), i.e. 2501 (kJ/kg). i is also a specific enthalpy for moist air but having the heat of sublimation of water vapor as an enthalpy reference rather than h_v^{ref}.

When the Lewis number is unity, Eqn. 1 can be approximated as follows using the boundary layer analogy.

$$q''_{tot} \approx \alpha_d\Big((C_{p,a} + C_{p,v}\omega_a)T_a - (C_{p,a} + C_{p,v}\omega_{sat}(T_\delta))T_\delta + h_{sub}(\omega_a - \omega_{sat}(T_\delta))\Big) \tag{17}$$

This approximation is valid with negligible error if the Lewis number is close to one [12]. Therefore,

$$\begin{aligned} q''_{tot} &\approx \alpha_d\Big(h(T_a,\omega_a) - h_{v,sat}(T_\delta) + (h_{sub} - h_v^{ref})(\omega_a - \omega_{sat}(T_\delta))\Big) \\ &= \alpha_d(i(T_a,\omega_a) - i_{v,sat}(T_\delta)). \end{aligned} \tag{18}$$

3.2. Reformulation and linearization

The second step is to reformulate and approximate the nonlinear heat flux equations in the frost layer, i.e. Eqn. 9 and 15, to a linear form with respect to the enthalpy difference. Reformulation processes are different depending on reference models that are described in the following two sections (Section 3.2.1 and 3.2.2). We will come up with a very simple expression for the combined heat and diffusion equations in the frost layer through the reformulation process. An approximation method is described in Section 3.2.3.

3.2.1. Reformulation of the first order homogeneous ice formation model

Evaluating Eqn. 6 at $y = \delta$ leads to

$$\rho_v(\delta) = \rho_{v,sat}(T_p)\cosh(M\delta), \tag{19}$$

By plugging Eqn. 19 into 9, one can obtain the following expression.

$$q_{tot}^{''} = \frac{k_{fr}}{\delta}(T_\delta - T_p) + \frac{Dh_{sub}}{\delta}(\rho_{v,sat}(T_\delta) - \rho_{v,sat}(T_p)). \tag{20}$$

Applying the mean value theorem and enthalpy to 20 results in

$$q_{tot}^{''} = \frac{k_{fr} + h_{sub}D\frac{d\rho_{v,sat}}{dT}(T^{**})}{\delta\frac{di_{v,sat}}{dT}(T^*)} \times (i_{v,sat}(T_\delta) - i_{v,sat}(T_p)) \tag{21}$$

for some $T^*, T^{**} \in (T_p, T_\delta)$.

3.2.2. Reformulation of the zeroth order homogeneous ice formation model

From boundary conditions at the frost surface layer, it is clear that

$$\begin{aligned} m_\rho^{''} &= D\frac{d\rho_{v,sat}}{dT}(\delta)\frac{dT}{dy}(\delta), \\ q_{tot}^{''} &= (k_{fr} + h_{sub}D\frac{d\rho_{v,sat}}{dT}(T_\delta))\frac{dT}{dy}(\delta). \end{aligned} \tag{22}$$

After manipulations of Eqn. 15 with Eqn. 22, Eqn. 15 can be reformulated as follows.

$$T_\delta = -\frac{m_\rho^{''}h_{sub}}{2k_{fr}}\delta + \frac{q_{tot}^{''}}{k_{fr}}\delta + T_p. \tag{23}$$

Solving the ordinary differential equation of Eqn. 13 under water vapor boundary conditions of Eqn. 4 results in the following water vapor distribution inside the frost layer.

$$\rho_v(y) = \frac{m_\rho^{''}}{2D\delta}y^2 + \rho_{v,sat}(T_p). \tag{24}$$

Evaluation of Eqn. 24 at $y = \delta$ leads to the expression of densification rate for the zeroth order model as follows.

$$m_\rho^{''} = 2\frac{D}{\delta}(\rho_{v,sat}(T_\delta) - \rho_{v,sat}(T_p)) \tag{25}$$

Substituting $m_{\rho}^{''}$ in Eqn. 23 with Eqn. 25 leads to exactly the same equation of Eqn. 20, and hence the expression of Eqn. 21 is also valid for the zeroth order homogeneous model.

3.2.3. Linearization approach

The two derivatives in Eqn. 21 are approximated as

$$\begin{aligned} \frac{d\rho_{v,sat}}{dT}(T^{**}) &\approx \frac{\rho_{v,sat}(T_{\delta}^{-}) - \rho_{v,sat}(T_p)}{T_{\delta}^{-} - T_p}, \\ \frac{di_{v,sat}}{dT}(T^{*}) &\approx \frac{i_{v,sat}(T_{\delta}^{-}) - i_{v,sat}(T_p)}{T_{\delta}^{-} - T_p}. \end{aligned} \tag{26}$$

where T_{δ}^{-} is the frost surface temperature calculated at the previous computation time step. For this calculation, the saturation curve of $i_{v,sat}$ is obtained using psychrometric relations (ASHRAE [15]) along with Eqn. 16.

By the approximation, the expression for heat flux through the frost layer, i.e. Eqn. 21, becomes

$$q_{tot}^{''} \approx \frac{k_{eq,fr}}{C^{*}\delta}(i_{v,sat}(T_{\delta}) - i_{v,sat}(T_p)) \tag{27}$$

where

$$k_{eq,fr} = k_{fr} + h_{sub}D\frac{\rho_{v,sat}(T_{\delta}^{-}) - \rho_{v,sat}(T_p)}{T_{\delta}^{-} - T_p}, \tag{28}$$

$$C^{*} = \frac{i_{v,sat}(T_{\delta}^{-}) - i_{v,sat}(T_p)}{T_{\delta}^{-} - T_p}. \tag{29}$$

Note that Eqn. 27 is valid regardless of the reference models.

3.3. Final form of simplified model

Since the forms of Eqn. 18 and Eqn. 27 provide a way to construct a thermal network, one can solve $q_{tot}^{''}$, $i_{v,sat}(T_{\delta})$ without any iterations as follows which are our final model.

$$q_{tot}^{''} = \frac{i(T_a, \omega_a) - i_{v,sat}(T_p)}{R_a^{*} + R_{fr}^{*}} \tag{30}$$

and

$$i_{v,sat}(T_{\delta}) = \frac{R_a^{*}}{R_a^{*} + R_{fr}^{*}} i_{v,sat}(T_p) + \frac{R_{fr}^{*}}{R_a^{*} + R_{fr}^{*}} i(T_a, \omega_a) \tag{31}$$

where $R_a^{*} = 1/\alpha_d$ and $R_{fr}^{*} = C^{*}\delta/k_{eq,fr}$.

Once $q_{tot}^{''}$ and $i_{v,sat}(T_{\delta})$ are calculated at each time step, T_{δ} can be determined from a correlation for $i_{v,sat}(T_{\delta})$ which can be easily developed using

psychometrics and Eqn. 16. Then, the mass flux of water vapor from the air side to frost surface can be calculated from Eqn. 10. The densification rate for the frost layer is calculated by either Eqn. 11 or 25 depending on the reference model. T_a and ω_a for the next downstream control volume can be calculated using energy and water vapor mass balances, and the frost thickness and density can be updated for the next time step using Eqn. 12. Correlations from the literature for frost thermal conductivity, diffusivity and convective heat transfer coefficient are employed to update parameters of Eqn. 30 and 31 (see Section 4 for descriptions for correlations). The above procedure is repeated for a predefined simulation period. The overall solution process for a control volume of our simplified and baseline approaches is depicted in Fig. 2. Note that the simplified modeling approach only differs in calculating T_δ (3rd to 5th block) while correlations for parameters in the 2nd block and models for water vapor flux to the frost surface and densification rate in the 6th block are the same for both approaches.

In the diagram, there are a few points to be mentioned for clarifying the frost surface temperature calculation for the proposed solution approach.

- T_δ is a variable to be calculated at each time step (see 5th block).
- To calculate T_δ, resistances in the 3rd block (or Eqn. 31) should be defined at each time step which require T_δ^- as shown in Eqn 27.
- Since T_δ^- is defined as the previously calculated frost surface temperature, i.e. $T_\delta^-(k) := T_\delta(k-1)$, an initial guess for T_δ^- at time zero should be specified.
- We assigned the initial guess as $T_\delta^-(t=0) = T_p + 10^{-2}(^oC)$ in the first block because it should be very close to the initial plate surface temperature.
- T_δ^- is not used for the reference solution approach.

3.4. Comments on simplified modeling approach

The presented model has been derived for a flat plate heat exchangers. However, the approach can be directly applied to more complicated heat exchanger geometries with a small modification of air side thermal resistance. This paper also includes a simplified model for a fin and tube heat exchanger, but it is described in the Appendix due to a large number of equations.

4. RESULTS AND DISCUSSION

This section provides result comparisons between the proposed model, reference models and experimental data available from the literature. Model behaviors for cold plates are first investigated and results are shown in Section 4.1 and 4.2. Comparisons for a more realistic case, a finned-tube heat exchanger in which frost accumulation interacts with a fan, is provided in Section 4.3.

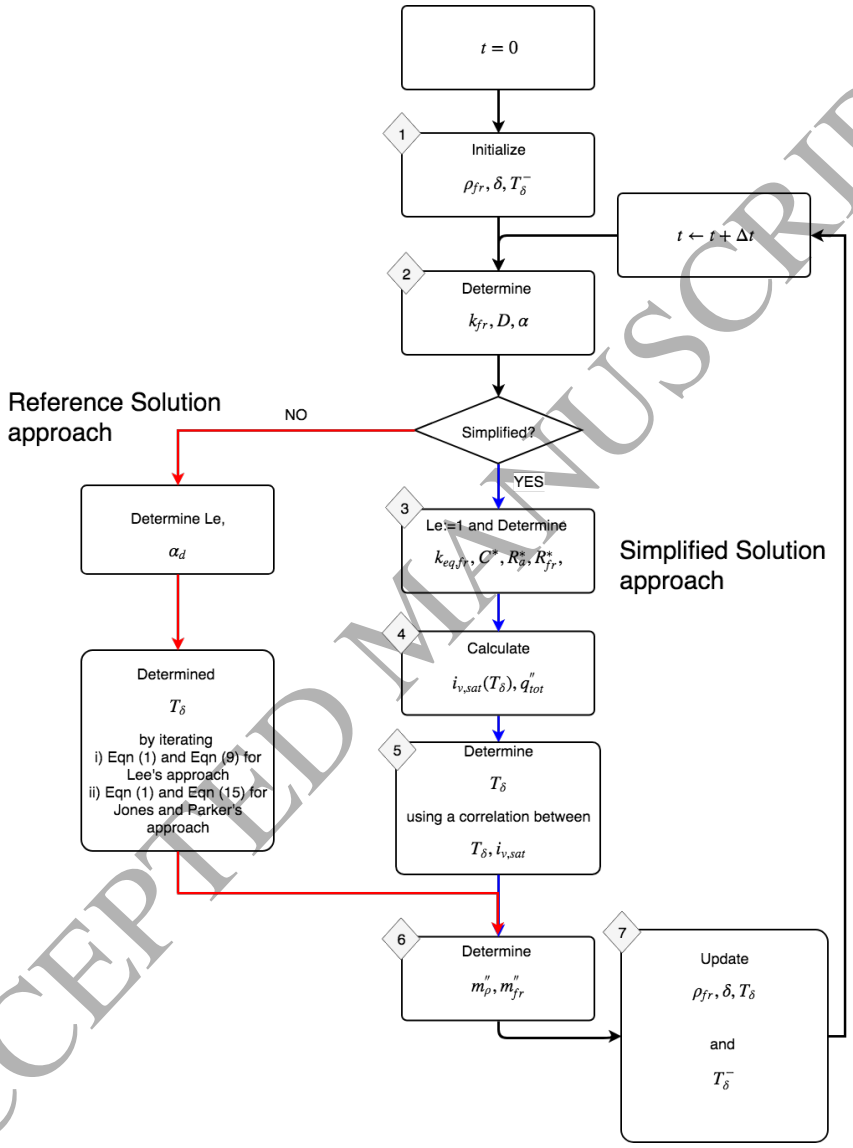

Figure 2: Solution process of a simplified model for one control volumne (flat plate heat exchanger)

The initial conditions for frost thickness and density are important and should match the actual initial conditions from the data for the models. The papers associated with the baseline models (Lee, and Jones and Parker) did not specify nor describe how they determined the initial conditions. In order to be consistent with those papers, we parametrically adjusted the initial conditions for our implementation of the reference models so that our reference model predictions matched those of the papers. For consistency, we used the same initial conditions of density and thickness for both the simplified model and reference models.

4.1. Results comparisons with Lee's data for a cold plate

The evaluation of the proposed simplified model, i.e. Eqn. 30 and 31, is performed by comparing the predicted frost thickness and frost surface temperature with those of the reference model and experimental data available from the literature (Lee et. al. [3]). In the test, the temperature of a flat plate, air temperature, humidity and velocity were regulated. For more detailed descriptions of the experimental setup, see [3].

The evaluation of the reference model follows the Lee's solution approach which is shown as the "Reference Solution approach" in Fig. 2. For each control volume and time step, the reference model, i.e. Eqn. 1, 8 and 9, was solved using the nonlinear equation solver *fsolve* in Matlab [16]. Frost density and thickness were updated at each time step based on a solution for frost surface temperature. CoolProp [17] was used to calculate properties of dry and moist air, and correlations for the diffusion coefficient, thermal conductivity of frost layer, the Lewis number, and air side heat transfer coefficient presented in [3] were applied. A 10 sec time step was employed.

On the other hand, the evaluation of the simplified model follows the "Simplified Solution approach" in Fig. 2. The same correlations and models for frost deposit and denstification rate presented in [3] were applied.

Fig. 3 shows comparisons of frost layer thickness and surface temperature under a frost condition. Air velocity, air temperature, air humidity and plate temperature are 1 m/s, 25 ^oC, 70 % and -15 ^oC, respectively.

There are some differences in predictions between the reference and simplified model resulting from simplifying assumptions. However, the discrepancies are in an acceptable range (up to 7% relative error in frost thickness) and it is evident that the simplified model captures the most significant dynamics of frost accumulation even compared to measurements.

To identify error sources, another simulation of the reference model with the Lewis number of unity was carried out. In this study, air conditions were varied and result comparisons are shown in Fig. 4. The results were almost identical to those of the proposed model (relative errors for the frost thickness and deviation of the frost surface temperature from the evaporator surface temperature are no more than 2 % and 3 % respectively), and thereby we conclude that the differences between the simplified and reference models are due to the assumption in the proposed model of $Le = 1$. The results imply that the linearization

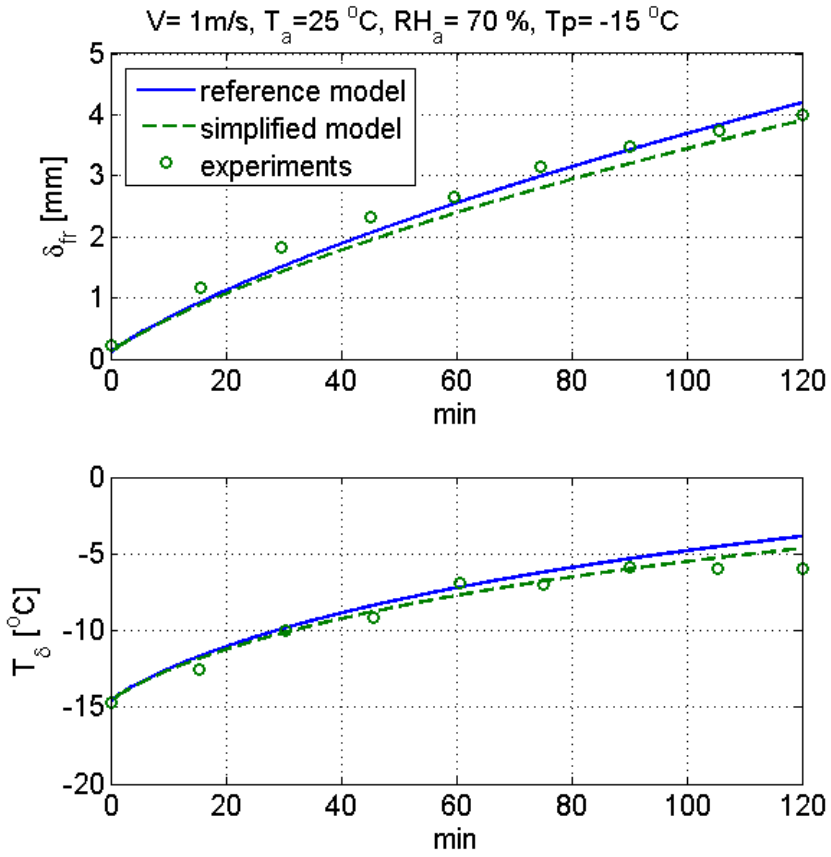

Figure 3: Comparisons of the simplified model with Lee's model and experimental data

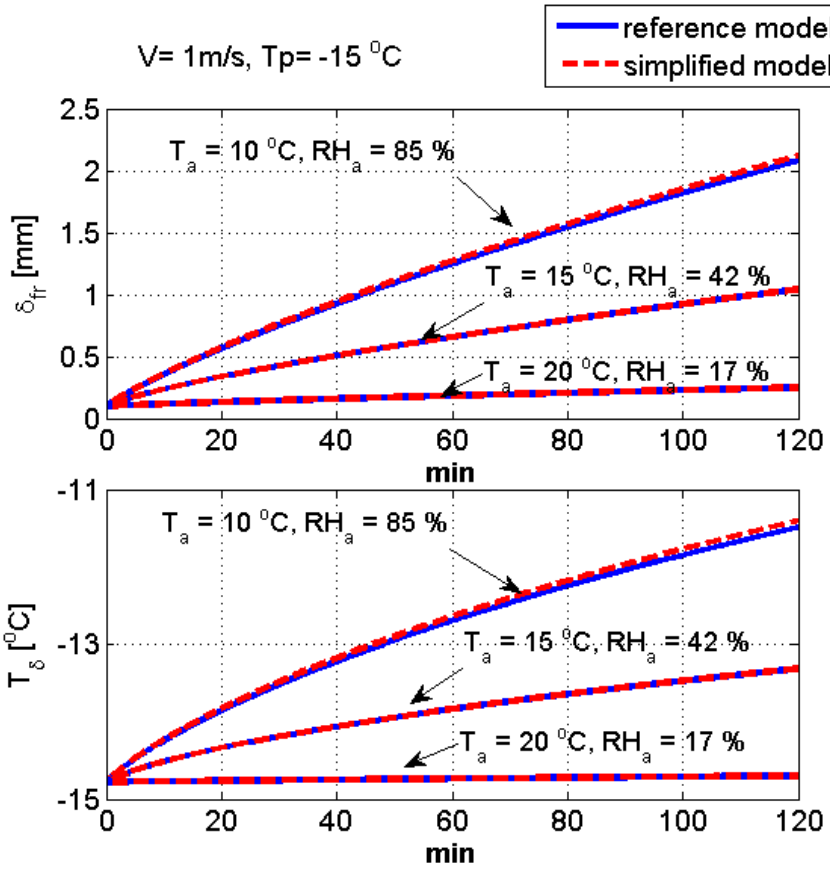

Figure 4: Comparisons of the simplified model with Lee's model under differeint air conditions

Table 1: Comparison of simulation times

	Lee's Model	Present Model
Computation time (sec)	24.36	1.55

approach to estimate derivatives of saturated properties of water vapors, i.e. Eqn. 26, does not introduce a significant approximation error.

Table. 1 compares simulation times for the two models for the 2-hr simulation period. The simplified model reduces the computation time by about a factor of 15 compared to the reference model.

Table 2: Boundary conditions (Jones and Parker)

Boundary Conditions	$T_a[^oC]$	$\omega_a[kg/kg]$	$T_p[^oC]$	$V[m/s]$
Case 1	21.85	0.0106	-18.15	2.57
Case 2	22.85	0.0117	-8.15	2.92

Table 3: Comparison of simulation times

Computation time (sec)	Jones and Parker's Model	Present Model
Case 1	38.61	2.46
Case 2	44.14	2.41

4.2. Results comparisons with Jones and Parker's data for a cold plate

The proposed simplified model is compared with Jones and Parker's model and experimental data from their paper [1]. The same numerical experiment described in the last section was used in simulation. Boundary conditions for tests are summarized in Table 2 and the duration of the tests is 180 min. In this case study, correlations of frost conductivity, diffusivity and air side heat transfer coefficient presented in [1] are employed for both models. Fig. 5 shows comparisons of the proposed model (dashed lines) with the reference model (solid lines) and measurements (dots).

It is not clear what causes differences between the predictions of the reference model and measurements due to lack of explanation in the reference paper. Nonetheless, the discrepancies are not significant. The last sub-figure in Fig. 5 shows an interesting behavior of the proposed model which under-predicts heat flux at the beginning while it eventually over-predicts the heat flux. This is because of the higher Lewis number, i.e. $Le = 1$, of the proposed model. Since increased Lewis number implies lower mass transfer coefficient α_d for the proposed model, predictions of heat and water vapor transfer from air to frost layer are lower than those of the reference model at the beginning. This can be confirmed with the slower frost growth of the proposed model as shown in Fig. 5. In addition, since the thermal resistance of the reference model increases faster than that of the proposed model due to faster frost accumulation, the proposed model eventually over-predicts the heat flux compared to the reference model. However, the simplified model actually agrees better with the experimental data.

Comparisons of simulation times for the two models for the 180-min simulation period are summarized in Table. 3. The simplified model reduces the computation time by about a factor of 15 to 20 compared to the reference model.

4.3. Results comparisons with Silva's data for a fan-supplied fin-and-tube heat exchanger

The modeling scheme is applied to a fin and tube heat exchanger operating with a fixed speed fan. Experimental results are taken from Silva et. al. [7]. The geometry information for the evaporator is summarized in Table 4. For

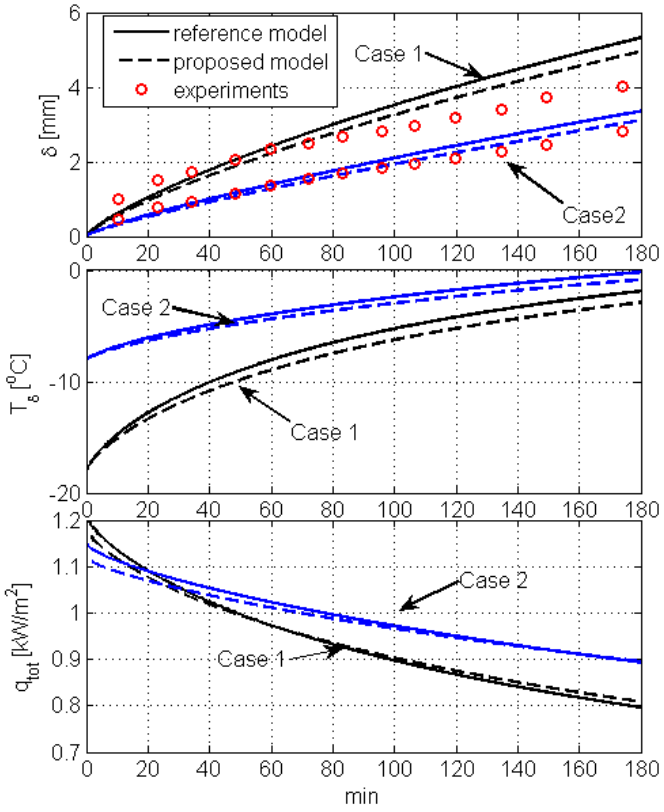

Figure 5: Comparisons of the simplified model with Jones and Parker's model and experimental data

Table 4: Summary of evaporator geometry

Type	Finned circular tube cross-flow
Width of the HX	320 mm
Height of the HX	152 mm
Depth of the HX in airflow direction	45 mm
Tube outer diameter	10 mm
Fin thickness	0.2 mm
Fin density	4 fins/cm
Number of tube rows	2
Number of tubes per row	6
Transversal tube pitch	25 mm
Longitudinal tube pitch	22 mm

more detailed descriptions of the heat exchanger and experimental setup, refer to the reference paper.

Because of long mathematical descriptions of the reference and simplified models, they are provided in the Appendix (Section 6.2). A brief outline of the approaches is as follows. A control volume was made for each tube of the heat exchanger. It is assumed that inlet air conditions for each row are uniform. Uniform frost thickness on both tubes and fins is further assumed, and the superheated refrigerant zone is neglected for model simplicity. Mass and energy balances are applied to air side and frost layer of the control volume and overall fin efficiency is utilized to take the fin effect into account. The ϵ-NTU method is employed for both sensible and latent heat transfers. The boundary analogy is used to calculate the convective mass transfer coefficient. For the frost layer, the first order homogeneous ice formation model (Lee's approach) is adopted according to the reference paper. A resulting baseline model forms essentially the same model structure for flat plate cases. Therefore, to construct a simplified model, the same numerical approach described in Section 3 was applied to the baseline model.

It should be noted that for the finned tube heat exchanger case, unlike flat plate cases, there is an interaction between frost accumulation and the fan characteristic because growth of frost narrows down air flow passages leading to a reduced air flow rate. Fig. 6 shows simulation results of the proposed model for frost thickness and dimensionless free flow passage area, i.e. A_{free}/A_{face} (see the Appendix), under a frosting condition; inlet air temperature, air humidity and tube surface temperature are 2 (^oC), 80 (%) and -10 (^oC), respectively. Reduction of flow area passage is clearly seen in the first sub-figure due to frost accumulation as shown in the second sub-figure. About half of the air flow passage is blocked after 40 min, and only 20% of the air flow passage under dry conditions is available after 1 hr. The second sub-figure shows that the frost layer of the first tube row is thicker than that of the second row. This is due to higher humidity of the air inlet steam for the first row which creates a higher potential for the water vapor transfer.

Results comparisons for the corresponding air pressure drop, air flow rate and (total) cooling capacity between experiments, proposed and reference models are shown in Fig. 7. Both models predict behaviors of those quantities within ± 5 $[Pa]$, ± 20 $[m^3/h]$ and ± 70 $[W]$ error bounds. As mentioned, the discrepancy between the proposed and reference model is due to the Lewis number assumption.

Comparison of computation times is summarized in Table 5. The proposed model is around 3.22 times faster than the reference model. Although the corresponding time saving is still significant, the relative speed is significantly reduced compared with that of flat plate cases which are around a factor of 15. This is due to additional nonlinear algebraic equations that calculate air flow rate using an updated frost thickness and fan curve for each time step. Since this paper is about heat exchanger modeling rather than system modeling, it is of interest to know the time saving without the flow rate iteration. To do this we re-ran both models with previously calculated flow rates as if flow rates

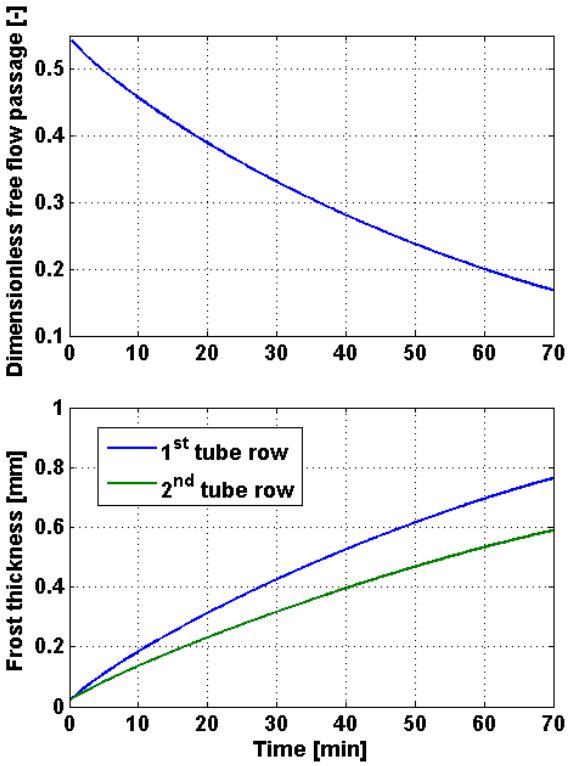

Figure 6: Calculated free flow passage and frost thickness with the simplified model

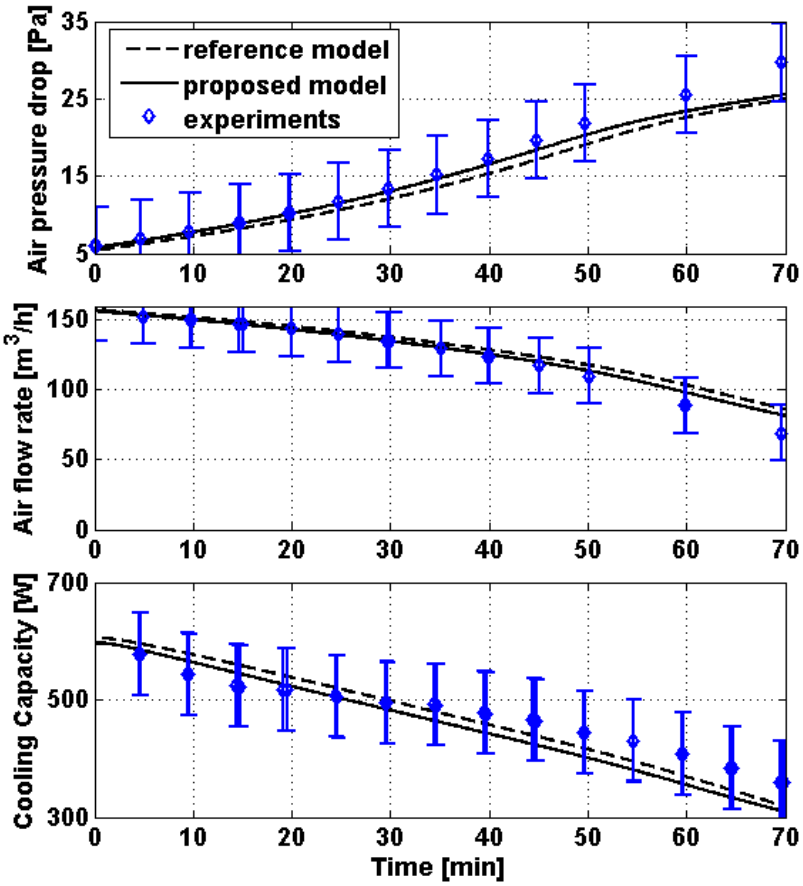

Figure 7: Comparisons of reference and simplified models with experimental data (fin-and-tube): The error bars indicates ± 5 $[Pa]$, ± 20 $[m^3/h]$ and ± 70 $[W]$ error bounds.

Table 5: Relative simluation speed of the proposed model compared with Silva's model (see Appendix)

case	speed [-]	time saving [%]
with flow rate iter.	3.22	68.95
w/o flow rate iter.	8.00	87.49

are known: evaporators having variable speed fans could be the case. In this scenario, the proposed model is 8 times faster than the reference model.

5. CONCLUSIONS

A numerically efficient modeling approach that avoids iterations in predicting the performance of evaporators under frosting conditions was derived and demonstrated. The methodology was developed based on reformulation of more detailed reference models using an enthalpy potential and linear approximation method. It was shown that the approximation strategy is accurate over a wide range of frosting conditions. The proposed model was compared with reference models and experimental data from the literature for flat plate and finned tube heat exchangers. It is 8 to 20 times faster than the reference models but with comparable accuracy.

6. APPENDIX

6.1. Nomenclature for Appendix

A_{HT} **:** heat transfer area per tube row (m^2)

A_{flow} **:** minimum free flow area per tube row (m^2)

A_{face} **:** heat exchanger face area per tube row, i.e. $W \times S_T$ (m^2)

d_o **:** outer tube diameter (m)

FD **:** fin density (#/m)

G_{max} **:** mass flux at the maximum air velocity point of HX (kg/s)

N_R **:** number of tube rows of HX (-)

$N_{T/R}$ **:** number of tubes per each HX row (-)

S_L **:** longitudial pitch (m)

S_T **:** transverse pitch (m)

t_f **:** fin thickness (m)

W **:** width of heat exchanger (m)

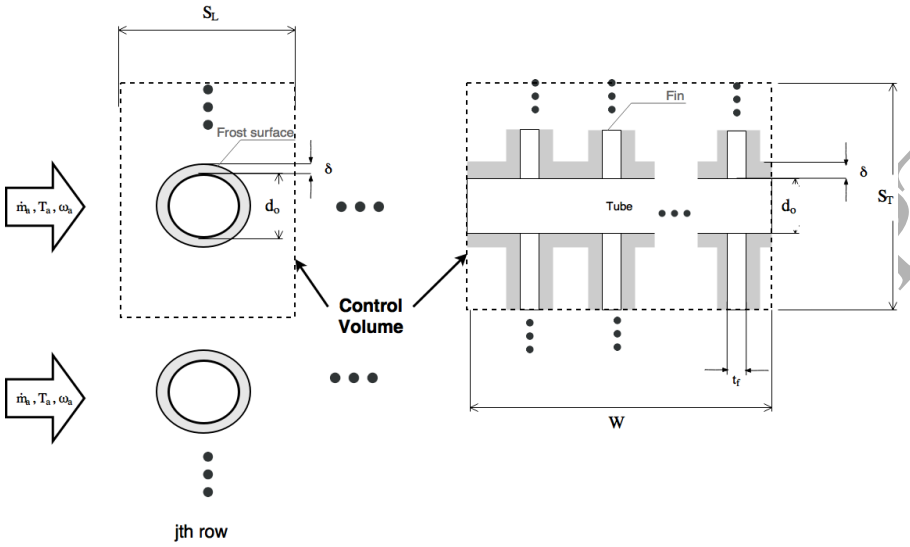

Figure 8: Schematic of a finned tube evaporator under frosting conditions and control volume

ϵ_s : sensible HX effectiveness (-)

ϵ_l : latent HX effectiveness (-)

ϵ^* : HX effectiveness w.r.t. enthaply potential (-)

η_o : overall fin efficiency (-)

$\rho_{a,i}$: air density at the inlet of tube row (kg/m^3)

$\rho_{a,o}$: air density at the outlet of tube row (kg/m^3)

σ : the ratio of the minimum free-flow area of the finned passages to the frontal area of the heat exchanger (-)

6.2. Simplified modeling approach applied to a finned tube heat exchanger

Fig. 8 shows a schematic diagram of a finned tube cross flow heat exhanger. There are N_R-number of tube rows along air flow direction and $N_{T/R}$-number of tubes in each row. A control volume was made over one of tubes at the j^{th} row having the volume of $S_T \times S_L \times W$. The air inlet conditions to the HX are represented as T_a, ω_a and $\dot{m}_a$. Note that $\dot{m}_a$ represents the air mass flow rate for a control volume, and hence a total mass flow rate of air can be obtained by multiplying $N_{T/R}$. Since the reference paper [7] does not provide a complete set of equations, such as updating rules for frost areas and some correlations, other papers were also utilized to establish the baseline models.

6.2.1. Assumptions

The following assumptions were employed from the reference paper [7] for modeling frosting finned-tube heat exchanger, in addition to the assumptions listed in Section 2.

- inlet air temperature and humidity are uniform for any row of a heat exchanger.
- refrigerant is two phase throughout a tube pass
- curvature of frost layer on tube is negligible

The assumptions above are mainly for simplicity of formulation by reducing the number of control volumes but can be relaxed without difficulties.

6.2.2. Heat and mass transfer equation in air side

The air side heat transfer equation is adopted from [7] as follows.

$$q''_{tot} = \frac{1}{A_{HT}}\Big(\epsilon_s \dot{m}_a C_{p,a}(T_a - T_\delta) + h_{sub}\epsilon_l \dot{m}_a\big(\omega_a - \omega_{v,sat}(T_\delta)\big)\Big) \tag{32}$$

where ϵ_s and ϵ_l represent sensible and latent effectiveness, respectively, expressed as follows.

$$\epsilon_s = 1 - \exp^{-\frac{\eta_o \alpha A_{HT}}{\dot{m}_a C_{p,a}}} \tag{33}$$

$$\epsilon_l = 1 - \exp^{-\frac{\eta_o \alpha_d A_{HT}}{\dot{m}_a}} \tag{34}$$

A_{HT} and η_o are the heat transfer area (or surface area) inside the control volume and the overall fin efficiency, respectively. Since frost thickness varies with time, they need to be updated at each computation step. The following geometric relations between the area and thickness are used for the update.

$$\begin{aligned} A_{fin} &= 2\left(S_L S_T - \pi(d_o{+}2\delta)^2/4\right) \times FD \times W \\ A_{base} &= \pi(d_o{+}2\times\delta) \times (W - (t_f{+}2\delta) \times FD \times W) \\ A_{HT} &= A_{fin} + A_{base} \end{aligned} \tag{35}$$

For the calculation of sensible convective heat transfer coefficient, correlations of Wang et. al. [18] that provide Colburn j factor are used. The minimal flow area is updated using the following relation.

$$A_{flow} = (S_T - (d_o + 2\delta)) \times (W - (t_f{+}2\delta) \times FD \times W) \tag{36}$$

The boundary layer analogy is used to calculate mass transfer coefficient as $\alpha_d = \frac{\alpha}{C_p Le^{2/3}}$, and correlations in [10] are used for calculating the overall fin efficiency.

Since the total heat flux from air to frost layer in Eqn. 32 relies on both temperature and humidity potential differences, the concept of enthalpy potential difference described in Section 3.1 is used based on the assumption of unity Lewis number. Using Eqn. 16, Eqn. 32 can be approximated as follows.

$$q''_{tot} \approx \frac{\dot{m}_a \epsilon^*}{A_{HT}} \left(i(T_a, \omega_a) - i_{v,sat}(T_\delta) \right) \tag{37}$$

where $\epsilon^* = \epsilon_l = \epsilon_s = 1 - \exp^{-\frac{\eta_o \alpha_d A_{HT}}{\dot{m}_a}}$.

6.2.3. Heat and mass transfer in frost layer

Due the assumption of the negligible curvature of frost layer, Eqn. 2 and 3 that describe heat and mass transfers in the frost layer also hold for a finned tube HX[2]. Therefore, the linear approximation method described in Section 3.2 can be directly applied as follows.

$$q''_{tot} \approx \frac{k_{eq,fr}}{C^* \delta} (i_{v,sat}(T_\delta) - i_{v,sat}(T_p)). \tag{38}$$

For the definition of the equivalent thermal conductivity, that considers heat generation due to the deposition of water vapor inside of the frost layer, see Eqn. 27.

6.2.4. Heat transfer equation in refrigerant side

In the reference paper [7], refrigerant and tube surface are considered to be the same due to a strong thermal coupling (or a relatively small thermal resistance) between them. However, for generalization, it is worthwhile to distinguish between them as follows. The corresponding heat transfer equation is

$$q''_{tot} = \alpha_r (T_p - T_r), \tag{39}$$

where T_r is refrigerant temperatures and α_r is an overall heat transfer coefficient between the tube (outside) surface and refrigerant.

Since the heat flux is dependent on the temperature potential difference, it is not compatible with Eqn. 37 and 38 which use enthalpy potentials. However, using the same methodology described in Section 3.2, Eqn. 39 is approximated with enthalpy potential as follows.

$$q''_{tot} \approx \frac{\alpha_r}{C^*_r} (i_{v,sat}(T_p) - i_{v,sat}(T_r)) \tag{40}$$

where

$$C^*_r = \frac{i_{v,sat}(T_p) - i_{v,sat}(T_r)}{T_p - T_r}. \tag{41}$$

[2]Here, we adopt the first order homogeneous ice formation model according to the reference paper [7].

6.2.5. Combined linearized model

Eqn. 37, 38 and 40 form a standard thermal network structure in which $i_{v,sat}(T_\delta), i_{v,sat}(T_p)$ and q''_{tot} can be calculated explicitly as follows.

$$q''_{tot} = \frac{i(T_a,\omega_a) - i_{v,sat}(T_r)}{R^*_a + R^*_{fr} + R^*_r} \tag{42}$$

and

$$\begin{aligned} i_{v,sat}(T_\delta) &= \frac{R^*_a}{R^*_a + R^*_{fr} + R^*_r} i_{v,sat}(T_r) + \frac{R^*_{fr} + R^*_r}{R^*_a + R^*_{fr} + R^*_r} i(T_a,\omega_a) \quad (43)\\ i_{v,sat}(T_p) &= \frac{R^*_a + R^*_{fr}}{R^*_a + R^*_{fr} + R^*_r} i_{v,sat}(T_r) + \frac{R^*_r}{R^*_a + R^*_{fr} + R^*_r} i(T_a,\omega_a) \end{aligned}$$

where

$$\begin{aligned} \mathrm{R}^*_a &= \frac{A_{HT}}{\dot{m}_a \epsilon^*} \quad (44)\\ R^*_{fr} &= \frac{C^*\delta}{k_{eq,fr}} \\ R^*_r &= \frac{C^*_r}{\alpha_r} \end{aligned}$$

As mentioned, the reference paper [7] provides only the tube (outside) surface temperature rather than refrigerant temperature and flow conditions. Therefore, for the case study of Section 4.3, we equate T_r to T_p and R^*_r to zero in Eqn. 43.

6.2.6. Frost growth

Once T_δ is calculated, densification rate and the mass flux of water vapor from the air to frost surface are calculated using (11) and

$$m''_{fr} = \frac{\epsilon_l \dot{m}_a}{A_{HT}} (\omega_a - \omega_{v,sat}(T_\delta)). \tag{45}$$

The frost thickness and density are updated for the next time step using Eqn. (12).

6.2.7. Pressure drop and mass flow rate

The fan performance curve (a typical light commercial axial fan) was obtained from the reference paper [7].

The pressure drop across the coil is calculated using [18] by

$$\Delta P = \frac{G^2_{max}}{2\rho_{a,i}} \Big(f \frac{A_{HT}}{A_{flow}} \frac{\rho_{a,i}}{\rho_m} + (1+\sigma^2)(\frac{\rho_{a,i}}{\rho_{a,o}} - 1) \Big). \tag{46}$$

where f is the friction factor obtained from the literature.

6.2.8. Correlations

For the effective diffusion coefficient of water vapor in the frost layer, the following equations are used [10, 6].

$$D = D_a \frac{\epsilon}{\tau} \tag{47}$$

$$\tau = 1 + \sqrt{\frac{\rho_{fr}}{\rho_{ice}}} \tag{48}$$

$$\epsilon = 1 - \frac{\rho_{fr}}{\rho_{ice}} \tag{49}$$

where ϵ and τ are the porosity and tortuosity of the frost layer. The thermal conductivity of the frost layer is determined by [19]

$$k_{fr} = 1.202 \cdot 10^{-3} \cdot \rho_{fr}^{0.963}. \tag{50}$$

6.2.9. Solution procedures for reference and simplified models

Fig. 9 shows the solution procedure for the proposed simplified modeling approach. A description for each solution step is:

1. Update minimum flow and heat transfer areas per each row using Eqn. 35 and 36, and calculate air flow rate using Eqn. 46 and a fan curve [7].
2. Start a loop from the 1st row of HX with air stream inlet boundary conditions of T_a and ω_a.
3. Calculate air side, frost layer and refrigerant side thermal resistances (with respect to enthalpy potential differences) using Eqn. 44.
4. Determine total heat flux and frost surface temperature using the linear thermal network model Eqn. 42.
5. Obtain frost and densification rates using Eqn. 45 and 11.
6. Calculate exit air temperature and humidity using energy and mass balances for air side, and update frost thickness and density using Eqn. 12.
7. Repeat steps from 3 to 7 with updated inlet air conditions for the other rows of HX.
8. After the final row is calculated, move to the next time step.

For the reference model, the steps from 3 and 4 are replaced by a step that solves a set of nonlinear algebraic equations of Eqn. 32, 9 and 39.

7. NOMENCLATURE

C_p **:** specific heat (J/kg-K)

D **:** (effective) diffusion coefficient considering porosity and tortuosity (m^2/s)

h **:** a specific enthalpy of moist air used in developing the psychrometric chart (ASHRAE) (J/kg)

h_{sub} **:** enthalpy of sublimation of water (J/kg)

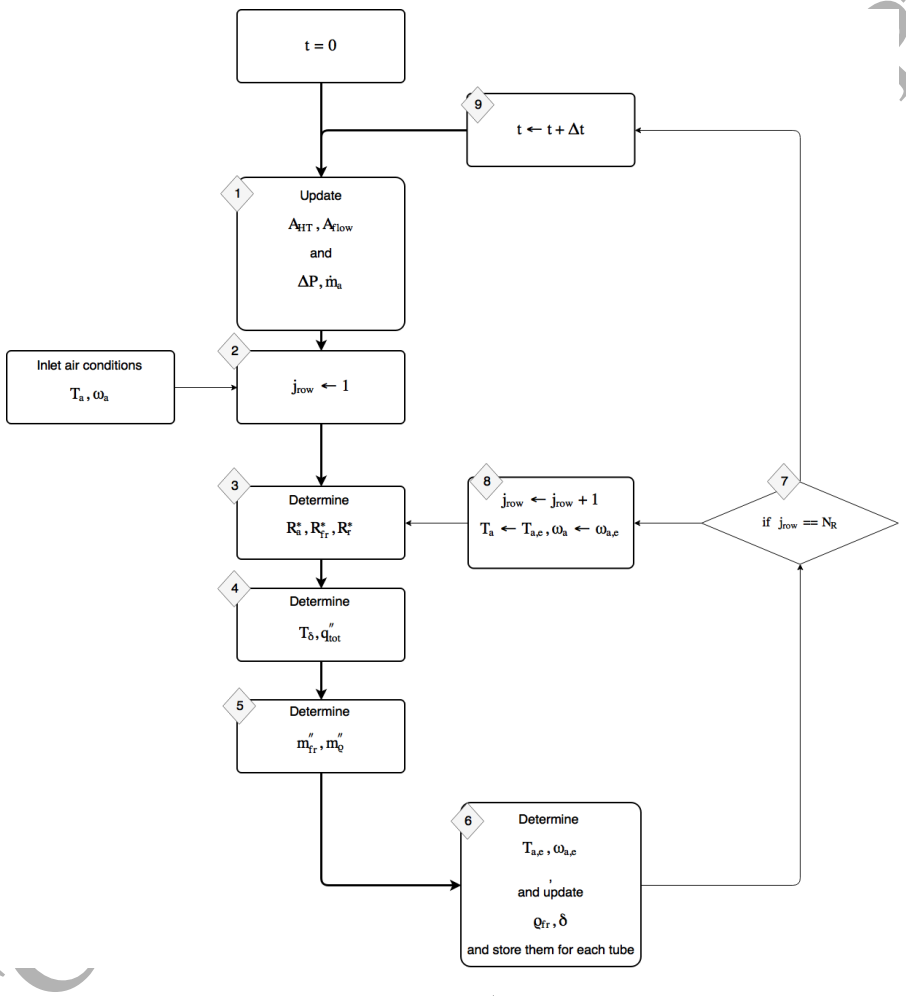

Figure 9: Solution process of a simplified model (finned tube heat exchanger under a fixed speed fan)

h_v^{ref} : a reference specific enthalpy of water vapor (J/kg)

h_v : a specific enthalpy of water vapor (J/kg)

i : a specific enthalpy of moist air having h_{sub} as reference

k : thermal conductivity (W/m-K)

k_{eq} : equivalent thermal conductivity of a frost layer (W/m-K)

$m^{''}$: mass flux (kg/m^2-s)

$m_{fr}^{''}$: mass flux of water vapor from the air to frost surface (kg/m^2-s)

$m_{\rho}^{''}$: mass flux for densification of frost layer (kg/m^2-s)

$q^{''}$: heat flux (W/m^2)

$q_{tot}^{''}$: total heat flux, sensible and latent (W/m^2)

R^* : thermal resistance w.r.t. enthalpy potential difference (m^2-s/kg)

T : temperature (^oK)

T_δ : surface temperature of a frost layer for a control volume at a time (^oK)

T_p : plate surface temperature or tube (outside) surface temperature for a control volume at a time (^oK)

α : convective heat transfer coefficient (W/m^2-K)

α_m : convective mass transfer coefficient (m/s)

α_d : $\alpha_m \times \rho_{air}$ (kg/m^2-s)

δ : frost thickness at a time (m)

κ : absorption rate (1/sec)

ρ : density (kg/m^3)

ω : humidity ratio (kg/kg-air)

Subscript

a : air

fr : frost

p : plate

r : refrigerant

sub : sublimation

v : vapor

v, sat : saturated vapor

REFERENCES

References

[1] B. Jones, J. Parker, Frost formation with varying environmental parameters, Journal of Heat Transfer 97 (2) (1975) 255–259.

[2] S. N. Kondepudi, D. L. O'Neal, Performance of finned-tube heat exchangers under frosting conditions: I. simulation model, International Journal of Refrigeration 16 (3) (1993) 175–180.

[3] K.-S. Lee, W.-S. Kim, T.-H. Lee, A one-dimensional model for frost formation on a cold flat surface, International Journal of Heat and Mass Transfer 40 (18) (1997) 4359–4365.

[4] D.-K. Yang, K.-S. Lee, S. Song, Modeling for predicting frosting behavior of a fin–tube heat exchanger, International journal of heat and mass transfer 49 (7-8) (2006) 1472–1479.

[5] C. Tso, Y. Cheng, A. Lai, An improved model for predicting performance of finned tube heat exchanger under frosting condition, with frost thickness variation along fin, Applied Thermal Engineering 26 (1) (2006) 111–120.

[6] S. Padhmanabhan, D. Fisher, L. Cremaschi, E. Moallem, Modeling non-uniform frost growth on a fin-and-tube heat exchanger, international journal of refrigeration 34 (8) (2011) 2018–2030.

[7] D. L. Da Silva, C. J. Hermes, C. Melo, First-principles modeling of frost accumulation on fan-supplied tube-fin evaporators, Applied Thermal Engineering 31 (14) (2011) 2616–2621.

[8] K.-S. Lee, S. Jhee, D.-K. Yang, Prediction of the frost formation on a cold flat surface, International journal of heat and mass transfer 46 (20) (2003) 3789–3796.

[9] J.-S. Kim, K.-S. Lee, S.-J. Yook, Frost behavior on a fin considering the heat conduction of heat exchanger fins, International Journal of Heat and Mass Transfer 52 (11) (2009) 2581–2588.

[10] D. Seker, H. Karatas, N. Egrican, Frost formation on fin-and-tube heat exchangers. part imodeling of frost formation on fin-and-tube heat exchangers, International Journal of Refrigeration 27 (4) (2004) 367–374.

[11] M. Kandula, Frost growth and densification on a flat surface in laminar flow with variable humidity, International Communications in Heat and Mass Transfer 39 (8) (2012) 1030–1034.

[12] J. W. Mitchell, J. E. Braun, Principles of heating, ventilation, and air conditioning in buildings, John Wiley and Sons., Inc., New York, NY, 2013.

[13] F. C. McQuiston, J. D. Parker, Heating, ventilating, and air conditioning: analysis and design, John Wiley and Sons., Inc., New York, NY, 1982.

[14] S. Sherif, S. Raju, M. Padki, A. Chan, A semi-empirical transient method for modelling frost formation on a flat plate, International Journal of Refrigeration 16 (5) (1993) 321–329.

[15] A.S.H.R.A.E., Fundamentals, Vol. 111, 2001.

[16] M. U. Guide, The mathworks, Inc., Natick, MA 5 (1998) 333.

[17] I. H. Bell, J. Wronski, S. Quoilin, V. Lemort, Pure and pseudo-pure fluid thermophysical property evaluation and the open-source thermophysical property library coolprop, Industrial & engineering chemistry research 53 (6) (2014) 2498–2508.

[18] C.-C. Wang, K.-Y. Chi, C.-J. Chang, Heat transfer and friction characteristics of plain fin-and-tube heat exchangers, part ii: Correlation, International Journal of Heat and mass transfer 43 (15) (2000) 2693–2700.

[19] C. T. Sanders, Frost formation: The influence of frost formation and defrosting on the performance of air coolers, Ph.D. thesis, TU Delft, Delft University of Technology (1974).